Turkish Journal of Electrical Engineering & Computer Sciences

http://journals.tubitak.gov.tr/elektrik/

Research Article

Turk J Elec Eng & Comp Sci
(2022) 30: 805 – 817

doi:10.3906/elk-2106-153

# On an electrostatic micropump with a rigorous mathematical model

**Ibrahim EFE, Fatih DIKMEN*, Yury TUCHKIN**
Department of Electronics Engineering, Gebze Technical University, Kocaeli, Turkey

**Received:** 30.06.2021 • **Accepted/Published Online:** 29.12.2021 • **Final Version:** 21.03.2022

**Abstract:** The novel electrostatic micropump model for applications such as in biomedical drug delivery is presented. The geometrical arrangement of the coupling rigid electrodes lets us exploit our mathematically rigorous boundary integral equation formulation and its solution. Thus, the charge densities involving the fringe effects on the plates are obtained by means of analytical regularization method (ARM) constructed for annular strips earlier. The efficiency of the constructed method is demonstrated with respect to the direct integral equation solvers implemented via the entire domain Galerkin method and point matching. The main physical characteristics of the suggested system and their deviation from that of infinitely large plane approximation are discussed.

**Key words:** Electrostatic pump, numerical simulation, integral equation, analytical regularization, orthogonal polynomials method

## 1. Introduction

Dynamical microfluid systems based on a combination of mechanical and electrical phenomena are commonly met in biomedical micropump systems [1–3]. Among them, electrostatically-actuated microelectromechanical systems (EA-MEMS) are well-known as structurally simple and operationally flexible [4]. We suggest a displacement type EA-MEMS with rigid electrodes [5], which, without flexible membranes [6, 7], do not require the involvement of the deflection phenomenon in their analysis. Then, this EA-MEMS implementation is solely dependent on the attraction of the charges of the coupling plates [6, 7]. Our model is elaborated via the first kind boundary integral equation (BIE) formulation of the Laplace Equation [8, 9]. Such BIE analyses are quite common among investigations on complex MEMS constructions [10]. We solved, thus, obtained system of the integral equations by means of orthogonal polynomials methods (OPM) involving Chebyshev polynomials [12, 13], enhanced by analytical regularization method (ARM) [14].

The analytically regularized mixed boundary value problems (BVP) of Laplace equation on surfaces involving holes and spacing between them, like the plates of the micropump construction here, have been worked thoroughly by the end of last century. The foundations of well-conditioned solutions of these problems on the basis of dual series equations concerning the 2 and 3 dimensional (2 & 3D) boundaries osculating the separable coordinates are a result of these efforts and summarized in [15] at the beginning of 00's. The BVP on the 3D axially symmetrical surfaces satisfying Dirichlet boundary condition fall into the category that the ARM can be applied. The context of this category involves the parameterized boundaries in 2 & 3D, which need not to be coordinate surfaces, and it can be followed in the review paper [16] where ARM is limited to

*Correspondence: dikmen@gtu.edu.tr

its special case, i.e., semiinversion. The ARM installation used here was firstly introduced in [17] regarding 2D problems of wave scattering. The canonical integral equation (CIE) for ARM was discretized with dual series equations (DSE) rather than the OPM [12, 13]. The OPM for Dirichlet BVP is an entire domain Galerkin procedure where basis and testing functions are performed via Chebyshev polynomials of the first kind and the scalar product with corresponding weights and have been used with different nomenclature [18]. The infinite algebraic equation obtained, thus, is of the first kind as $Ax = b; x, b \in l_2$ in the space of numbers in computers, i.e. ,the space of square summable sequences. The truncated solutions of these algebraic systems are unstable with growing system dimensions, and the ARM defines $(I + H) = LAR$ with the well-known left $(L)$ and right $(R)$ hand regularizing operators of operator theory specified to the operators of the problem at hand in an invertible fashion [14, 19]. Here, $I$ is the unit, $H$ and $A$ are the compact operators in $l_2$ . After this operation, the resultant infinite algebraic system becomes the second kind in $l_2$ space: $(I + H)y = g; y, g \in l_2$ where $y = R^{-1}x, g = Lb$ as the numerical stability is manifested by the uniformly bounded condition numbers of these algebraic systems as their dimensions tend to infinity. Having the Dirichlet BVP for Helmholtz equation uniquely and equivalently reduced to this numerically stable algebraic system by means of OPM and ARM, well-conditioned numerical performance of the 2D problem in [20] followed the works with the same CIE in [21–23] which elaborated 3D axially symmetrical annular strips, with similarly successful demonstration of their performances. This approach proved useful for the open toroidal screens on which the Dirichlet BVP for the Laplace equation has been solved very recently [9]. The Dirichlet BVP of Laplace equation has also been treated with ARM for toroidal closed screens, and for a 3D shell of revolution on the basis of Fourier series equations in [9] for the former and DSE in [8] for the latter. The plate surfaces of the micropump construction here, differ than those surfaces, being open and having no common points with the symmetry axis (Figure 1 and Figure 2). The singularity extraction, which is in the heart of the ARM analysis in those works is the same for BVP of the Laplace and Helmholtz equations and is simply inherited here to form the corresponding CIE in the way described below. In this work, we exploit this whole know-how on extracting the characteristics of an electrostatic micropump.

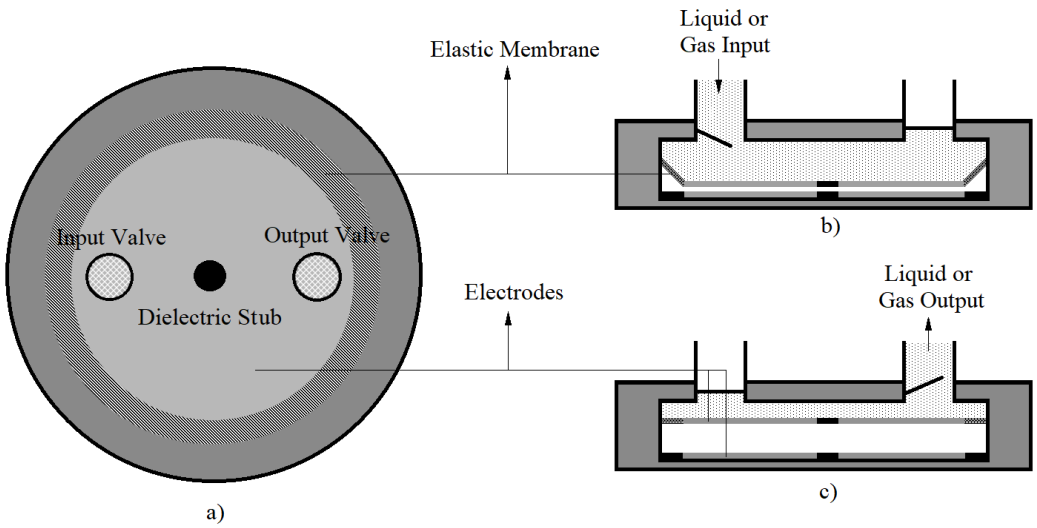


**Figure 1**. Sketch of electrostatic micropump structure: a)Top view, b)Sucking mode, c)Pumping mode.

The sketch of the suggested design is shown in Figure 1, and its operational principle is basically as follows: The forces between the rigid parallel plates are produced by the electrostatic attraction of the electrodes caused by the application of switching voltages [3, 24]. The inner holes of rings in Figure 2 are filled with dielectric stub discs in Figure 1. With that setting, the lower electrode is fixed to the bottom of the chamber. The upper rigid electrode is mounted to the chamber walls with a flexible dielectric ring at its relaxed (unstretched) position when no electrostatic force is applied on. This dielectric spring stretches as electrodes approach each other under the attractive electrostatic forces. In this way, the chamber can be filled with liquid through the inlet into the reservoir situated above the moving electrode, and the fluid flows out through the outlet. The amount of the flow in the unit of time depends on the surface area of the plates, the distance between them, and the driving voltage.

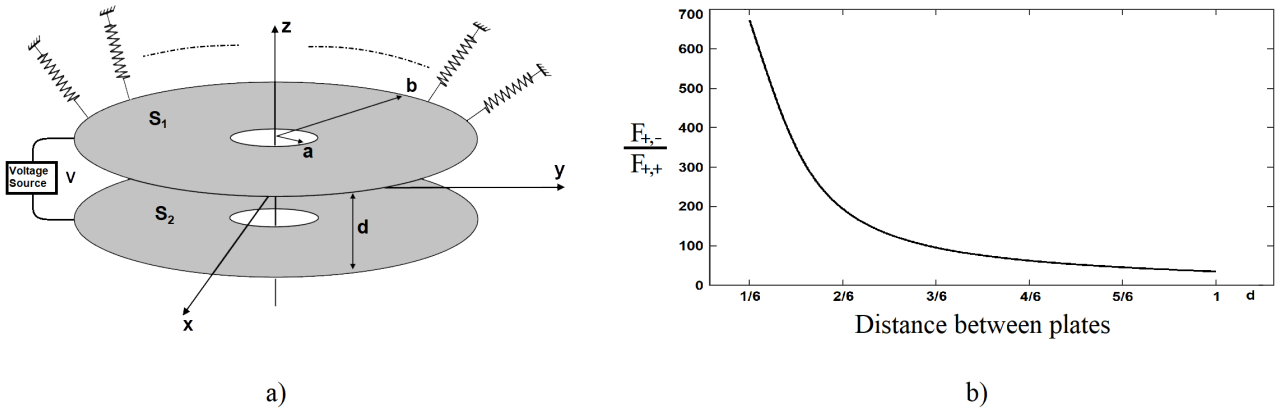


**Figure 2**. a)Geometrical structure of plate-spring model b)Ratio of normalized forces - attraction and repulsion

### 1.1. The force between the plates

It is common practice to calculate the charge on the parallel plates in such EA-MEMS installations as a constant on infinite plates, i.e., neglecting the fringing electrostatic field and the curvature of the equipotential lines. In this approximation, the following simple formula for the force magnitude is used [25],

$$F = \frac{\varepsilon A V^2}{2d^2} \tag{1}$$

where $\epsilon$ is the dielectric permittivity of the medium, $d$ is the distance between the plates, $V$ is the potential difference between the plates, and $A$ is the area of the electrodes. In fact, the force between the plates with fixed potentials is the gradient of the stored electrostatic energy $W_e$, resulting in (1) under the idealization mentioned above [26]. When the fringing quantities are not neglected the force is the gradient of $W_e$, we have an integral representation throughout the portion of the space "$v$" occupied by the device.

$$\mathbf{F} = \nabla W_e = \mathbf{z}\frac{\varepsilon}{2}\int_v \left[\frac{\partial}{\partial z}|\mathbf{E}|^2\right] dv, \quad \mathbf{E} = -\nabla U \tag{2}$$

The potential distribution between the plates $U$ here is calculated rigorously throughout the boundary integral equation written on the geometric support of the charged electrodes, formulation of which is given in the next section.

## 2. Mathematical and computational models of the potential distribution in space with the Dirichlet boundary conditions, including the ARM

In Figure 2, since the driving voltage $V$ is fixed on electrodes and the system is axially symmetrical, $U$ does not vary with azimuthal angle, and the dimension of the problem depends on $\rho$ and z in cylindrical coordinates. Due to the same symmetry, the total forces along any radial direction are equal to zero. Therefore, the only variation of the forces are along $z$ axis in the region of the device.

The $U(\mathbf{q})$ observed at point $\mathbf{q}$ exists due to the surface charge density $\zeta_j(\mathbf{q})$ on the points $\mathbf{q}$ of the electrode numbered $i$ $(i = 1, 2)$. The posing of the BVP below is based on the version of ARM similar to that used for solving the Dirichlet problem for Laplace equation in presence of an open shell of revolution in [8] and for both open and closed toroidal surfaces in [9]. The corresponding BVP is classically formulated [27] (i) for the potentials satisfying homogenous Laplace equation $\nabla^2 U(\mathbf{q}) = 0$, (ii) with the Green's function $G(\mathbf{q},\mathbf{p}) = 1/(4\pi|\mathbf{q} - \mathbf{p}|)$, (iii) as the total potential converges uniformly to zero at infinity: $U(\mathbf{q} \to 0)$ as $|\mathbf{q}| \to \infty$, (iv) under Dirichlet boundary conditions on the surfaces of the electrodes in the $\lim_{h\to+0} U_i(\mathbf{p}\pm hn_p)+V_i(\mathbf{p}) = 0, i = 1, 2$ where $\mathbf{n_p}$ is the surface normal at point $\mathbf{p}$, (v) with the Meixner's edge conditions requiring the field energy integral to be finite in any confined spatial volume including the edges: $\int_v \left[|\nabla U|^2\right] dv < \infty$ leading us to a search of the unknowns of the integral representation in the form $\zeta_j(\mathbf{p}) = (d_{j1}(\mathbf{p})d_{j2}(\mathbf{p}))^{-1/2} h_j(\mathbf{p})$ where $d_{jk}, k = 1, 2$ are distances from the edges and $h_j(\mathbf{p})$ belongs to Hölder class on the surface. Since this integral representation is over the infinitely thin surfaces forming the geometrical support of the electrodes (Figure 2), the dimension of the integral representation of the potential over this surface in 3D domain will reduce one more, to lead a 1D integral representation of the potential distribution along the radial direction and, thus, the following integral equation:

$$\sum_{j=1}^{2} \int_S \zeta_j(\mathbf{p}) G(\mathbf{q}_i, \mathbf{p}) dS = -V(\mathbf{q}_i), \qquad \mathbf{q}_i \in C_i, \quad i = 1, 2 \tag{3}$$

(3) is elaborated in the same fashion given in [9, 21] with the following setting: Despite the azimuthal independence of the geometry and the excitation, substitution of the Fourier series expansions with respect to the azimuthal coordinate $\phi$ of all functions in (3), as in [9, 21], is appropriate due to the $2\pi$ - periodicity of the functions with respect to $\phi$. Evidently, the constant value of the right hand side of (3) results in the independence of all values in the equation, on $\phi$. Therefore, the equation is reduced to the so-called DC term, i.e., the only $m = 0$ term presented, where $m$ is the azimuthal index of the Fourier expansion. Both plates have their constant $z$- coordinate and the same inner and outer radii $a$ and $b$, respectively. To form the CIE, the points $\mathbf{p}$ on every plate are parameterized as

$$\mathbf{p}(v) = (z, \rho(v)) = (z, [(b - a)v + (b + a)]/2), \; b > a, \; v \in [-1, 1], \; \rho \in [a, b] \tag{4}$$

$$ds(\mathbf{p}(v)) = \rho(v)\rho'(v)dv$$

It is well known that the singular part of the Green's function of scalar Helmholtz equation consists of the Green's function of scalar Laplace equation $G(\mathbf{q}, \mathbf{p})$ given above. That is why the system (3) can be reduced to the following CIE, solution procedure of which is similar to the algorithm established for scalar waves satisfying

Helmholtz equation [21] and Laplace equation [9], on the parameters in (4).

$$\int_{-1}^{1}\left\{-\frac{1}{\pi}ln|u-v|+K_{ii}(u,v)\right\}\frac{m_i(v)}{\sqrt{1-v^2}}dv\ +\int_{-1}^{1}K_{ij}(u,v)\frac{m_j(v)}{\sqrt{1-v^2}}dv=b_i(u), \tag{5}$$

$$u\in[-1,1],\ i=1,2;\ j=2,1$$

In (5), the unknown $m_i(v)$ are smooth functions of at least the Hölder class, and all the kernels $K_{ij}$ are smooth functions too. When $i\neq j$ , the kernel of the second integral originates from the infinitely smooth function $G(\mathbf{q}_i,\mathbf{p}_j)$ , i.e., the source and the observation points are on the different plates. The Fourier coefficient $G_m^{ij}(z,\rho)$ for $m=0$ of the kernels in (3) in cylindrical coordinates $(\rho,\phi,z)$ is evidently the following:

$$G_0^{ij}(z,\rho)=\frac{1}{2\pi}\int_{-\pi}^{\pi}G(\mathbf{q}_i,\mathbf{p}_j)d\varphi=\frac{1}{8\pi^2}\int_{-\pi}^{\pi}\frac{d\varphi}{\sqrt{(z_i-z_j)^2+(\rho_i-\rho_j)^2+4\rho_i\rho_j\sin^2\left(\frac{\varphi}{2}\right)}} \tag{6}$$

As $i=j$ the kernel originating from $G(\mathbf{q}_i,\mathbf{p}_j)$ has the logarithmically singular kernel as in (5) - see details in [9, 21] and the next section. The Fourier-Chebyshev coefficients of the logarithmic singularity in (5) are known. This fact gives a possibility to construct the $L$ and $R$ regularizers of the equation (5) based on OPM technique as in [9, 21–23]. This construction leads to the infinite system of linear algebraic equations of the second kind with uniformly bounded condition numbers of the finite system matrices for the increasing to infinity of their truncation numbers (see-section 3).

An alternative and more compact way to view the singularity of this problem, the kernel in (5) is split with the help of the following relation [28, 29]:

$$G_0^{ij}(\rho(u),\rho(v))=\frac{1}{4\pi\sqrt{\rho(u)\rho(v)}}Q_{-\frac{1}{2}}(\chi(u,v)),\quad \chi(u,v)=\frac{\rho^2(u)+\rho^2(v)}{2\rho(u)\rho(v)} \tag{7}$$

where $G_0^{ij}$ is the Fourier coefficient of the $G(\mathbf{q}_i,\mathbf{p}_j)$ defined by (6). It is given in closed form (7) by means of the negative half-integer degree Legendre function of the second kind of order zero $Q_{-1/2}$, which is also known as a toroidal function [28–30]. In appendix A, we cast the corresponding series representation to enable the validation of the following:

$$Q_{-\frac{1}{2}}\left(\chi(v+\delta,v)\right)=-ln\delta+K_{ii}\left(v+\delta,v\right),\quad \delta=|u-v|, \tag{8}$$

where the function $K_{ii}(v+\delta,v)$ is more smooth including the vicinity of value $\delta=0$. To the knowledge of the authors, the way to (5) from (3) after substitution of (7) with appropriately scaling the equation by $\sqrt{\rho(u)}$ in a much explanatory fashion than the one obtained after cumbersome local singular expansion calculations given in [9, 21] is given here for the first time. The most natural way of solving equation in (5) is based on utilization of OPM involving Chebyshev polynomials of the first kind. The polynomials are orthogonal with the weight $(1-v^2)^{-1/2}$, which fits the Meixner edge condition pointing at the square root singularity at the edges for the new unknown charge density $\zeta_i(\mathbf{p}(v))\rho'(v)\sqrt{\rho(v)}=(1-v^2)^{-1/2}m_i(v)$ [9, 21]. Once $\zeta_i(\mathbf{p})$ are found after

solving $m_i(v)$ from (5), the distribution of the potential $U(\mathbf{q})$ at any point $\mathbf{q}$ in the space can be calculated as follows:

$$U(\mathbf{q}) = \sum_{i=1}^{2} \int_{S_i} \zeta_i(\mathbf{p}) G(\mathbf{q}, \mathbf{p}) ds(\mathbf{p}) \tag{9}$$

## 3. Results and discussion of numerical modelling

We start with Figure 3 demonstrating the numerical stability and the physical relevance of the used model in Figure 3.a. For comparision, we facilitate a direct solution of the same integral equation (3) with the method of moments using point matching (Appendix B). Both figures there to cast the drastic differences between the formulations with infinite matrix operators $A$, $A$ with point matching, and $(I + H)$. Notice that the solutions with operator $A$ correspond to the direct solution of the integral equation with the entire domain Galerkin method [18]. The relative error between the solutions at a certain truncation $N$ and $2N$, in $l_2$ norm in Figure 3a shows how fast the convergence with the lattermost operator is, while that of the first and second required much larger truncation numbers for the same accuracy (e.g., for relative error of $10^{-4}$, we observe the necessary system sizes as 28, 128, 16, respectively), which Figure 3b finds it questionable to happen. The condition numbers with increasing truncation numbers of the algebraic systems $A$, $A$ with point matching, and $(I + H)$ in Figure 3b are given. The accuracy of the solution obtained via $A$ cannot be improved by increasing the truncation number, since the exponential increase in the condition number of $A$ and $A$ with point matching means that the loss of accuracy in the solution is increasing. Roughly, in a computational environment with a mantissa length of 16 decimal figures, if condition numbers are greater or equal to numbers in order of $10^{16}$, all accuracy of the corresponding solution is lost [19]. With uniformly bounded condition numbers of $(I + H)$, increasing the truncation only leads to more accurate significant digits in the corresponding solutions. Therefore, such solutions can be obtained with predefined accuracy.

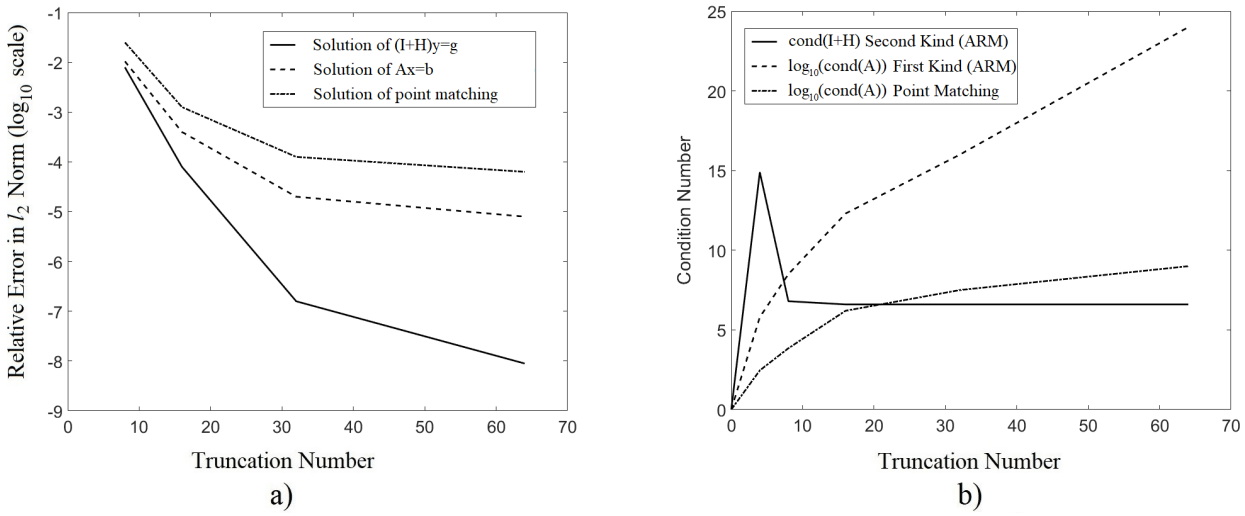


**Figure 3**. a)Convergence analysis b)Condition number

The physical characteristics of the pump model in Figure 1 and Figure 2 are exposed as the results of the charge and force distributions on the plates calculations, as well as the potential space distribution and the capacitance of the plate system. All physical and geometrical values below are normalized in order to be dimensionless ones. In particular, the outer radii of the both rings are equal to $R = 1$. Inner radii of the rings are equal to $r$ and given as fractions of $R$. The values of the forces and capacities are normalized according to formulae (10) and (11). Relative permittivity is set $\epsilon = 1$. The only possible value of the independent voltages on the plates is normalized as $V = 1$. Figure 4a and Figure 4b depicts the calculated surface charge density distributions on the plates as functions of $d$ with two possible voltage configurations ($V_{1,2}$=(+,-);(+,+)) (former case has a 2V difference between the plates, while the latter case has none). Figure 4c and Figure 4d demonstrates the spatial potential distribution of the $U$ around the plates.

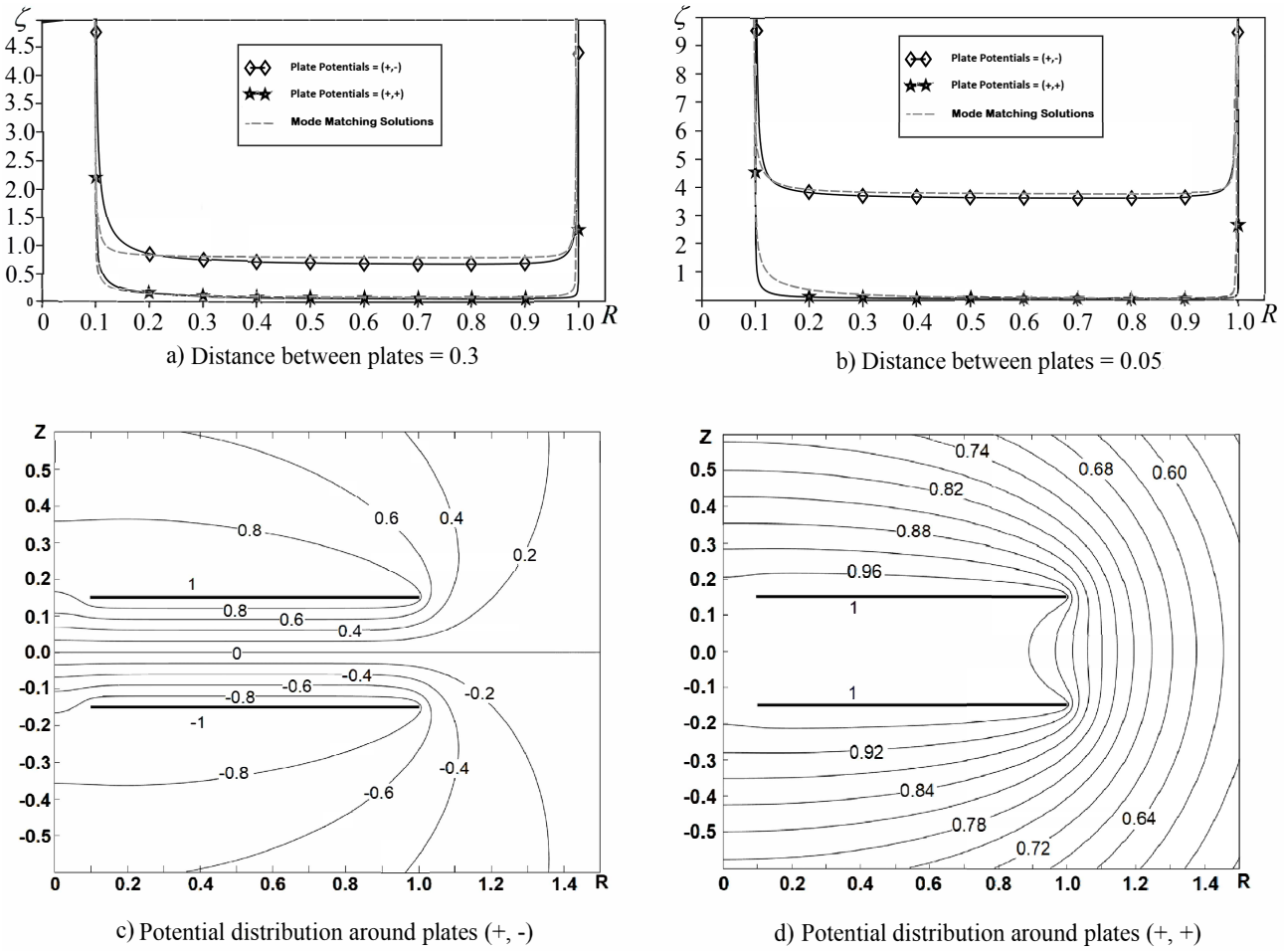


**Figure 4**. Charge and Potential distributions.

Aside the results of the employed rigorous algorithm, the point matching results are also depicted for a comparison exposing the relevance and the difference of both approaches. The point matching distributions depicted took twice the truncation number (N = 128) and, therefore, 8 times slower calculation by means of solving the corresponding linear algebraic systems. If we recall the convergence trends in Figure 3a, we observe

that the relative error of the point matching is larger at least of order $10^{-3}$ than the suggested method's at the truncation numbers pronounced. This also lies underneath the graphically observable differences in Figure 4a and Figure 4b between the surface charge densities obtained with both methods.

Figure 4a and Figure 4b show well-known square root singularity $\rho^{-1/2}$ of the charge densities, where $\rho$ is the distance from the observation point on the ring to its edge. As well, the charge density is nearly constant, and its value is close to that of the system of infinite plates when the observation point is far enough from the edges. The mentioned singularities predefine the spatial distribution of potential $U$. It is seen on Figure 4c and Figure 4d that the distribution of $U$ between the rings is similar to that for infinite plates when the observation point is on some distance from the edges. Nevertheless, the presence of the edges essentially influences the distribution around the plates and, consequently, on the capacitance of the system and the electrostatic forces applied to the plates. This effect is the reason why the forces and capacitances on Figure 5 depend on $d$ and are different from the corresponding approximative values.

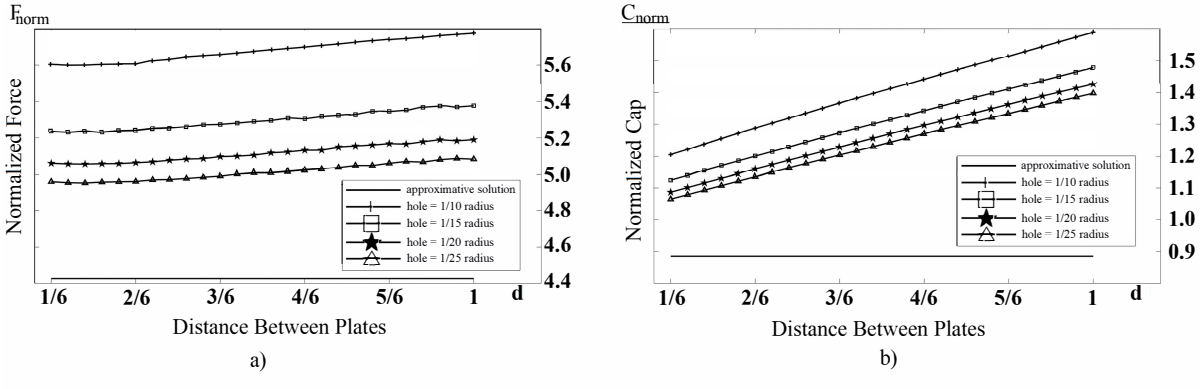


**Figure 5**. a)Normalized attraction forces $F_{norm}$ via distance between rings b)Normalized capacitances $C_{norm}$ via distance between rings

As seen in Figure 5a, when we apply the same potentials of the same sign to the plates, the charge density and, hence, the repulsion force is very small compared to the situation when the plates are charged with potentials of the opposite signs. This result led us to use the spring electrode model. The elastic membrane seen in Figure 1 constitutes the returning elastic force applied to the rigid movable plate. The normalized force applied to the rings is $F_{norm} = (d^2/V^2)F_z$ where $F_z$ is the modulus of $z$ component of the force in (1) and (2), see Figure 5a. In the formula (10), $C$ is the capacitance. Notations $F^e_{norm}$ and $F^a_{norm}$ correspond to exact solution explained above and approximative solution for infinite plates, respectively. Thus,

$$F^e_{norm} = \frac{d^2}{2}\frac{dC}{dz} \tag{10}$$

$$F^a_{norm} = \frac{\epsilon A}{2} \tag{11}$$

The approximated $C^a$ and exact value $C^e$ of $C$ are calculated as follows:

$$C^a = \frac{\epsilon A}{d} \tag{12}$$

$$C^e = \frac{\int_v \left[\epsilon |\nabla U|^2\right] dv}{V^2} \tag{13}$$

In Figure 5b the normalized capacitances $C_{norm} = (d/A)C$ are depicted correspondently to the cases in Figure 5a. In both figures, approximative values of $F_{norm}$ and $C_{norm}$ do not depend on the distance between the rings. In Figure 5a and Figure 5b, the results of exact calculations are performed, while the inner radii of the rings vary with certain proportions of the outer radii. These variances show that the normalized attractive and repulsive forces between the rings increase when the inner radii diminish. Thus, the accurate calculations show the essential influence of the parameter $d$. It means that this influence must be taken into account in design of a real pump.

## 4. Conclusion

Thus, axially symmetrical EA-MEMS structure is modeled as a system of parallel flat infinitely thin and perfectly conductive ring electrodes. For this aim, a rigorous and accurate method to the solution of the electrostatic actuated micropump model is suggested and solved with ARM in OPM version. The solution procedure is numerically stable, and it can be efficiently performed with any predefined accuracy [8, 14, 16]. Compared to the direct solution, using entire domain Galerkin method and point matching, the suggested solution was performed with much higher accuracy in much shorter calculation time. The method suggested herein provides the key approach to numerical analysis of a wide area of structures that can be modelled with parametrized boundaries in the way that ARM is useful for, which can cover rather complicated EA-MEMS constructions. In particular, the features of the method make it promising regarding simulations of much more general electrostatic problems. Such generalizations are supposed to be the subject of our future publications.

## 5. Appendix

### A. Logarithmic singularity of the associated legendre function of the second kind of order zero and degree (-1/2)

In addition to $\chi(u,v)$ defined in (7), let us introduce $R(u,v) = |\rho(u) - \rho(v)|$ and $S(u,v) = \dfrac{(\rho(u)+\rho(v))^2}{(\rho(u)^2+\rho(v)^2)^2}$.

As it is known [28, 29], $Q_{-1/2}(\chi) = \pi(2\chi)^{-1/2}{}_2F_1(3/4, 1/4; 1, 1/\chi^2)$ identity holds, where ${}_2F_1$ is the Gauss hypergeometric function. The two convergent power series expansions of two linearly independent homogenous solutions of corresponding differential equation for ${}_2F_1$ according to $1/\chi^2 \in [0,1]$ can be used as follows:

$$Q_{-1/2}(\chi) = \begin{cases} A(\chi), & \dfrac{1}{\chi^2} \in \left[0, \dfrac{1}{2}\right] \\ B(\chi) + ln(R)C(\chi), & \dfrac{1}{\chi^2} \in \left[\dfrac{1}{2}, 1\right] \end{cases} \tag{14}$$

The simplifications of the Gamma functions in corresponding series in [30] by Legendre duplication

formula lead to

$$A(\chi) = \frac{\pi}{\sqrt{2\chi}} \sum_{n=0}^{\infty} \left[ \frac{\left(\frac{1}{2}\right)_{2n}}{\left(2^n n!\right)^2} \left(\frac{1}{\chi^2}\right)^n \right] \tag{15}$$

$$\begin{aligned} B(\chi) = &-\frac{1}{2\sqrt{\chi}} \left( ln(S) \sum_{n=0}^{\infty} \left[ \frac{\left(\frac{1}{2}\right)_{2n}}{\left(2^n n!\right)^2} \left(1 - \frac{1}{\chi^2}\right)^n \right] \right) \\ &- \frac{1}{2\sqrt{\chi}} \left( ln(S) \sum_{n=0}^{\infty} \left[ \frac{\left(\frac{1}{2}\right)_{2n}}{\left(2^n n!\right)^2} \left(1 - \frac{1}{\chi^2}\right)^n \left( \psi\left(\frac{3}{4} + n\right) + \psi\left(\frac{1}{4} + n\right) - 2\psi\left(1 + n\right) \right) \right] \right) \end{aligned} \tag{16}$$

$$C(\chi) = -\frac{1}{\sqrt{\chi}} \sum_{n=0}^{\infty} \left[ \frac{\left(\frac{1}{2}\right)_{2n}}{\left(2^n n!\right)^2} \left(1 - \frac{1}{\chi^2}\right)^n \right] \tag{17}$$

where $(\cdot)_n$ is the Pochhammer symbol, and $\psi$ is the digamma function in (15)–(17). As $\delta$ in (8) approaches zero, $R$ also approaches zero, and $1/\chi^2$ approaches unity. With that in hand, the second line in (14) and considering the n=0 term in (17) enables the local singular structure given in (8) as the rest of (14) in its first and second lines are standing smooth enough for $K$ in (8).

### B. Point matching

For comparison of our results, we used the point matching method [11]. We solve the following equation to compare with the solution of (5) to obtain a matrix equation $Zx = V$

$$\frac{1}{4\pi} \sum_{j=1}^{2} \int_{a_j}^{b_j} \xi(\rho)\, Q_{-\frac{1}{2}}\left(\chi(\rho_i, \rho)\right) d\rho = -\sqrt{\rho_i} V_i \tag{18}$$

$$q_i \in C_i, \qquad i = 1, 2$$

in formula (18) unknown function can be defined as $\xi(\rho) = \zeta_i(\rho)\sqrt{\rho}$.

#### B.1. Nonself terms

For nonoverlapping segments separated by sufficient distance, we divide the two parallel radial strips of total length $2(b-a)$ into $N$ segments of width $\Delta_\rho$ with $N$ basis functions. $\Delta_\rho = \frac{2(b-a)}{N}$ we apply simple centroidal approximation to (18), which yields

$$Z_{mn} = \frac{\Delta_\rho}{4\pi} Q_{-\frac{1}{2}}\left(\chi(\rho_m, \varrho_n)\right) \tag{19}$$

where $\rho_m$ and $\varrho_n$ are the field and source positioned at the center of each segment. This formula is valid for matrix elements other than diagonal terms. Right hand side potential vector is $V_m = \sqrt{\rho_m}\, V_0$ ; where $V_0$ is the value of the potential specified to the corresponding plate.

### B.2. Self terms

For overlapping segments (diagonal terms), we need to consider the singularity of the kernel with small argument approximation [9]. We note that (19) is logarithmically singular when $\delta \to 0$

We can separate singular and smooth parts of DC term of Green's function in (7) scaled with the squareroot term in (7) similarly as in [9].

$$Z_{mm} = \lim_{\rho_m \to \varrho_m} -\frac{1}{4\pi} \int_0^{\Delta_\rho} Q_{-\frac{1}{2}} \left(\chi(\rho_m, \rho)\right) d\rho \tag{20}$$

$$Q_{-\frac{1}{2}} \left(\chi(\rho_m, \rho)\right) = \{S(\rho_m, \rho) + D(\rho_m, \rho)\} \tag{21}$$

$$S(\rho_m, \rho) = -\frac{1}{\pi} ln|\rho_m - \rho| + \frac{1}{\pi}(1 - ln2) \tag{22}$$

$$D(\rho_m, \rho) = -\frac{1}{2\pi} \left\{ ln \left( \frac{(b-a)^2}{\rho_m\, \rho} \right) + 2(1 - 4ln2) \right\} \tag{23}$$

$D$ and the second term in $S$ are the smooth parts of the kernel, which we can integrate numerically. But the first term, i.e., the logarithmically singular part in $S$, needs to be evaluated analytically. After some arithmetic operations [11] and substituting $\rho_m = \Delta_\rho/2$ and doing some simplification, the integral evaluates to

$$I = \int_0^{\Delta_\rho} ln|\rho_m - \rho|\, d\rho = \Delta_\rho \left(ln(\Delta_\rho) - ln2 - 1\right) \tag{24}$$

## References


[1] Bourouina T, Bosseboeuf A, Grandchamp J P. Design and simulation of an electrostatic micropump for drug delivery applications. Journal of Micromechanics and Microengineering 1999; 7 (3): 186–188. doi: 10.1088/0960-1317/16/11/028

[2] Mahija K, Pushpalatha BG, Jijesh JJ. MEMS based drug delivery system using micropump. International Journal of Electronics Signals and Systems (IJESS) 2013; 2 (3): 211-215. doi:10.47893/IJESS.2013.1108

[3] Cobo A, Sheybani R, Meng E. MEMS: Enabled drug delivery systems. Advanced Healthcare Materials 2015; 47 (7):969-982. doi: 10.1002/adhm.201400772

[4] Nisar A, Afzulpurkar N, Mahaisavariya B, Tuantranont A. MEMS-based micropumps in drug delivery and biomedical applications. Sensors and Actuators B: Chemical 2008; 130 (2): 917–942.10 doi:10.1016/j.snb.2007.10.064

[5] Zengerle R, Richter M. Simulation of microfluid systems. Journal of Micromechanics and Microengineering 1999; 412 (4): 192-204. doi: 10.1088/0960-1317/4/4/004

[6] Nemirovsky Y, Degani OB. A methodology and model for the pull-in parameters of electrostatic actuators. Journal of Microelectromechanical Systems 2001; 10 (4): 601-615. doi:10.1109/84.967384

[7] Maithripala DHS, Berg JM, Dayawansa WP. Control of an electrostatic MEMS using static and dynamic output feedback. Journal of Dynamic Systems Measurement and Control 2004; 127 (3): 443-450. doi:10.1115/1.1985443

[8] Panin S, Smith PD, Vinogradova ED, Tuchkin Yu A, Vinogradov SS. Regularization of the Dirichlet problem for Laplace's equation: surfaces of revolution. Electromagnetics, Taylor & Francis Online 2009; 29: 53–76.19 doi:10.1080/02726340802529775

[9] Tuchkin Yu A, Panin S, Efe İ, Dikmen F, Ünal İ et al. Electrostatic Problem for Toroid Surfaces; Analytical Regularization, 2021 International Applied Computational Electromagnetics Society (ACES) Online-Live, Interactive Symposium, August 1-5, doi: 10.1109/ACES53325.2021.00045

[10] Liu YJ. Dual BIE approaches for modeling electrostatic MEMS problems with thin beams and accelerated by the fast multipole method. Engineering Analysis with Boundary Elements 2006; 30 (11): 940– 948.22 doi:10.1016/j.enganabound.2006.04.010

[11] Gibson Walton C. The Method of Moments in Electromagnetics 3rd Ed, CRC Press

[12] Popov G. Ya. On the method of orthogonal polynomials in contact problems of the theory of elasticity. Journal of Applied Mathematics and Mechanic 1969; 33 (3): 503-517. doi:10.1016/0021-8928(69)90065-3

[13] Popov G. Ya. The axisymmetric mixed problem in the theory of elasticity for a hallow truncated circular cone. Journal of Applied Mathematics and Mechanics 2000; 64 (3): 413-424. doi:10.1016/S0021-8928(00)00064-2

[14] Tuchkin Yu A. On the Analytical Regularization Method in scattering and diffraction. In: Kobayashi K and Smith P D (editors). Advances in Mathematical Methods for Electromagnetics; Chapter 13 SciTech Publishing, 2020

[15] Vinogradov S, Smith P, Vinogradova E. Canonical problems in scattering and potential theory Part I: Canonical structures in Potential theory (Chapman & Hall/CRC, Boca Raton, FL, 2002).

[16] Nosich AI. The method of analytical regularization in wave-scattering and eigenvalue problems: Foundations and review of solutions. IEEE Antennas and Propagation Magazine 1999;41 (3):34.

[17] Tuchkin Yu A. Wave scattering by open cylindrical screens of arbitrary profile with Dirichlet boundary conditions. Soviet Physics Doklady 1985;30 (12):1027

[18] Butler CM. General Solutions of the Narrow Strip (and Slot) Integral Equations.- IEEE Transactions on Antennas and Propagation, Vol. AP-33, No. 10, October 1985

[19] Poyedinchuk Ye, Tuchkin Yu A, Shestopalov VP. , New Numerical – Analytical Methods in Diffraction Theory, Mathematical and Computer Modeling, Vol 32, 2000, 1029-1046

[20] Yiğit, H.; Dikmen, F. Analytical Regularization Method for Rigorous Diffraction Analysis of Knife Edges for TM Waves. Math. Comput. Appl. 2011, 16, 738-747. https://doi.org/10.3390/mca16030738

[21] Dikmen F, Karacuha E, Tuchkin Yu A. Scalar Wave Diffraction by a Perfectly Soft Infinitely Thin Circular Ring. Turkish Journal of Electrical Engineering and Computer Science 2001; 9 (2): 199-220

[22] Ozkan E, Dikmen F, Tuchkin Yu A. Scalar Wave Diffraction by Perfectly Soft Thin Circular Cylinder of Finite Length; Analytical Regularization Method, Elektrik, Turkish Journal of Electrical Engineering and Computer Science, Tubitak Doga Series, Vol 10, 2002, 459-472

[23] Dikmen F, Tuchkin Yu A. Analytical regularization method for electromagnetic wave diffraction by axially symmetrical thin annular strips, Turk J Elec Eng & Comp Sci, Vol.17, No.2, 2009, Tubitak, doi:10.3906/elk-0811-10

[24] Amirouche F, Zhou Y, Johnson T. Current Micropump Technologies and Their Biomedical Applications. Microsystem Technologies 2009; 15 (5): 647-666. doi:10.1007/s00542-009-0804-7

[25] Francais O, Dufour I, Sarraute E. Analytical static modelling and optimization of electrostatic micropumps. Journal of Micromechanics and Microengineering 1997; 7 (3): 183–185. doi:10.1088/0960-1317/7/3/027

[26] Cheng D. Field and Wave Electromagnetics 2nd Ed, Addison Wesley

[27] Colton D, Kress R. Integral Equation Methods in Scattering Theory.-Wiley, 1983.

[28] Cohl HS, Rau ARP, Browne DA, Tohline JE, Barnes EI et al. Useful alternative to the multipole expansion of 1/r potentials. Physical Review A 2001; 64 (5): doi:10.1103/PhysRevA.64.052509

[29] Vasiliev EN. Excitation of bodies of revolution, Moscow: Radio and Communication 1987; [in Russian]

[30] Nikiforov AF, Uvarov VB. Special Functions of Mathematical Physics 1988; Birkhauser